Journal of Power Sources 205 (2012) 252–263

Contents lists available at SciVerse ScienceDirect

Journal of Power Sources

journal homepage: www.elsevier.com/locate/jpowsour

Dynamic optimization under uncertainty of the synthesis/design and operation/control of a proton exchange membrane fuel cell system

Kihyung Kim*, Michael R. von Spakovsky, Meng Wang, Douglas J. Nelson

Center for Energy Systems Research, Department of Mechanical Engineering, Virginia Polytechnic Institute and State University, Blacksburg, VA 24061, USA

ARTICLE INFO

Article history:
Received 10 August 2011
Received in revised form 3 November 2011
Accepted 4 November 2011
Available online 11 November 2011

Keywords:
Proton exchange membrane fuel cell (PEMFC) system
Multi-level optimization
Physical decomposition
Uncertainty quantification
Response sensitivity analysis
Dynamic optimization

ABSTRACT

Proton exchange membrane fuel cell (PEMFC) systems with their own fuel conversion unit typically consist of a fuel processing subsystem, a fuel cell stack subsystem, a work recovery-air supply subsystem, and a power electronics subsystem. Since these subsystems have different physical characteristics, their integration into a single system level unit makes the optimization problem of synthesis/design and operation/control highly complex. Thus, dynamic system/subsystem/component modeling and highly effective optimization strategies are required. Furthermore, uncertainties in the results of system optimization can be affected by any number of sources of uncertainty such as the load profiles and cost models. These uncertainties can be taken into account by treating the problem probabilistically. The difficulty with doing this, particularly when large-scale dynamic optimization with a large number of degrees of freedom is being used, is that the traditional probabilistic approaches are simply too computationally intensive. This difficulty can be overcome by the use of approximate approaches such as the response sensitivity analysis (RSA) method based on Taylor series expansion. Thus, in this paper, a stochastic modeling and uncertainty analysis methodology for energy system synthesis/design and operation/control which uses the RSA method is proposed and employed for calculating the uncertainties on the system outputs. Their effects on the development and control optimization of a 5 kWe PEMFC system are assessed by taking the uncertainties into account in the objectives and constraints. It is shown that these uncertainties significantly affect the reliability of being able to meet certain constraints (e.g., that on the CO concentration) during the synthesis/design and operation/control optimization process.

1. Introduction

Fuel cells are promising candidates as alternative energy conversion devices for transportation, stationary power, and portable applications. Over the last several decades, there has been an ever increasing interest worldwide in the development and use of fuel cells because they provide an efficient, safe, and reliable power solution. However, although fuel cell systems (FCSs) exhibit these great benefits, there still exist a number of technical barriers which must be overcome such as material durability, reliable interfacing with conventional utility grids, commercial viability, etc. Furthermore, to realize such systems and the potential benefits, there is a need for optimal system synthesis/design and operation/control.

The optimal synthesis/design and operation/control of FCSs requires advanced techniques for being able to determine the syntheses/designs and dynamic operating stages of such systems, which make them technically and economically viable, because FCSs are highly non-linear systems that have a number of reliability issues (e.g., catalyst poisoning, structural degradation, and temperature and pressure limitations), which must be addressed in order to avoid system failures. FCSs typically consist of a fuel processing subsystem (FPS), a fuel cell stack subsystem (SS), a work recovery-air supply subsystem (WRAS), and a power electronics subsystem (PES). Only the first three of these are considered in this study. Since each subsystem has significantly different physical characteristics (i.e. thermodynamic, kinetic, geometric, temporal, etc.), their integration into a single optimal system renders the problems of dynamic system synthesis/design and operation/control to be highly complex. Moreover, it is also very important to synthesize/design and control the systems intelligently in order not only to avoid, as mentioned above, episodes of system failure but as well to obtain optimal system operation across an entire load spectrum both in terms of maximizing energy savings and minimizing environmental effects.

Conventional approaches for synthesis/design are based on a single, full load condition at steady-state. This can significantly simplify the system optimization problem involved. However, because the optimization reflects only a single condition, it may provide over-/underestimated solutions of synthesis/design and also lead to non-optimal solutions for operation/control. Therefore, with the

* Corresponding author. Tel.: +1 678 844 5554; fax: +1 678 844 6714.
E-mail address: kihyung.kim@ge.com (K. Kim).

0378-7753/$ – see front matter © 2011 Elsevier B.V. All rights reserved.
doi:10.1016/j.jpowsour.2011.11.014

Nomenclature

C	capital cost ($)
C_{dl}	double layer capacitance in cathode (F cm^{-2})
c_p	specific heat (kJ kmol^{-1} K^{-1})
$\dot{E}_{net}$	system net power generation (W)
$\dot{E}_{WRAS}$	motor parasitic power by WRAS (W)
$\vec{G}$	vector of inequality constraints
$\vec{H}$	vector of equality constraints
$[H^+]$	bulk flow proton concentration (mol cm^{-2})
$[H^+]_0$	reference proton concentration (mol cm^{-2})
j	cell current density (A cm^{-2})
j_r	reaction current density (A cm^{-2})
$\dot{m}$	mass flow rate (kg s^{-1})
n	number of electrons
$\dot{n}$	Molar flow rate (mol s^{-1})
p	pressure (bar)
P	power (W)
T	temperature (K)
$\dot{W}_M$	required load on motor (W)
$\dot{W}_E$	work recovered by expander (W)
$\dot{W}_C$	required work on compressor (W)

Greek letters

α	transfer coefficient
κ	specific heat ratio
λ	coupling function
η_i	system/component efficiency of i
η	voltage overpotential
ν	variance
δ	standard deviation

Superscripts

design	design case
in	inlet
out	outlet

exception of systems which always operate at a single load point, it is necessary to take into account part as well as full load conditions during the development phase of a system.

Another difficulty is that as energy systems become larger and more complex, the greater number of possible system configurations and technologies that could possibly meet the designer's objectives optimally increases greatly. In addition, the system may need to be developed taking into account both the transient and environmental effects on system performance. Thus, the difficulty of developing the entire system via the formulation of a single optimization problem in which the optimal synthesis/design and operation/control of the system are achieved simultaneously is great and rather problematic due to the complexities involved. These complexities are further heightened with the introduction of uncertainty quantification into the problem, transforming the problem from a purely deterministic one into a probabilistic one. Uncertainties, system complexity and non-linearity, and large numbers of decision variables quickly render the single optimization problem unsolvable by conventional single-level optimization strategies. They can, nonetheless, be handled by sophisticated multi-level optimization strategies (i.e., decomposition strategies). Decomposition breaks the large-scale optimization problem down into a set of approximately equivalent smaller optimization problems in order to facilitate the optimization procedure. Decomposition approaches are very effective for the optimization of dynamic systems which have highly nonlinear characteristics with a large number of degrees of freedom. In this research, physical

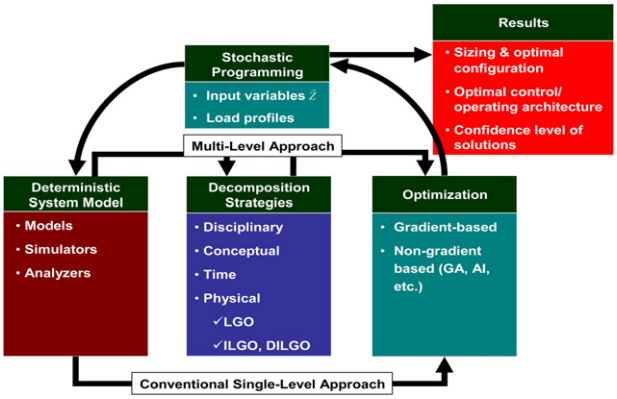

Fig. 1. Schematic of general modeling and optimization under uncertainty.

decomposition [1] is applied to the dynamic synthesis/design and operation/control optimization problem of a PEMFC system.

As to the uncertainties in the system synthesis/design and operation/control optimization results, these can be due to any number of sources, which can be categorized into direct ones such as those which result from computational errors and indirect ones such as those which result from a load profile and the fuel cost [2]. This study has focused on evaluating the uncertainties in system responses due to indirect uncertainty sources because the system optimization is significantly influenced by the load profile and cost information. Quantifying these uncertainties then becomes an important task in the development of the system. In this study, response sensitivity analysis (RSA) is employed and developed for use with dynamic energy system optimization. The load profile, fuel cost, and cost models are treated as probabilistic input values and uncertainties in the output results are determined.

Fig. 1 describes how all of the issues of system modeling, of multi-level optimization, of the choice of optimizer, of uncertainty quantification, etc. just outlined are integrated into a complete process, which simultaneously determines the dynamic system synthesis/design and operation/control optimization. The purpose of this research is to thoroughly study these issues and develop and apply appropriate techniques to address them in the development of a 5 kWe PEMFC system.

2. System description and modeling

2.1. PEMFC system description

Fig. 2 depicts the initial non-optimized configuration of a 5 kWe PEMFC system developed here, taking into account all of the equipment and recovery loops necessary for maximizing total system electrical efficiency. The main objective of the FPS is to provide the hydrogen rich gas required for the operation of the PEMFC stack. In particular, the FPS consists of three main steps; a desulfurization step as a fuel (e.g., natural gas) preparation process, a reforming step to reform the hydrocarbon fuel to a hydrogen rich gas, and a CO removal step to reduce the CO concentration level to less than 10 ppm. Organic sulfur contained in natural gas must be removed by the desulfurizer to prevent the detrimental effects on the catalysts in a typical PEMFC posed by the presence of sulfur.

For the reformer model, steam reforming technology is selected, and a steam generator and a combustor are introduced to support the steam-methane reformer (SMR). Reformate gas from the SMR usually contains between an 8 to 10% concentration of CO. It is necessary to reduce the CO concentration below 10 ppm for safe operation of the PEMFC system. To satisfy this requirement, a three-step CO removal unit is designed for this FPS which includes

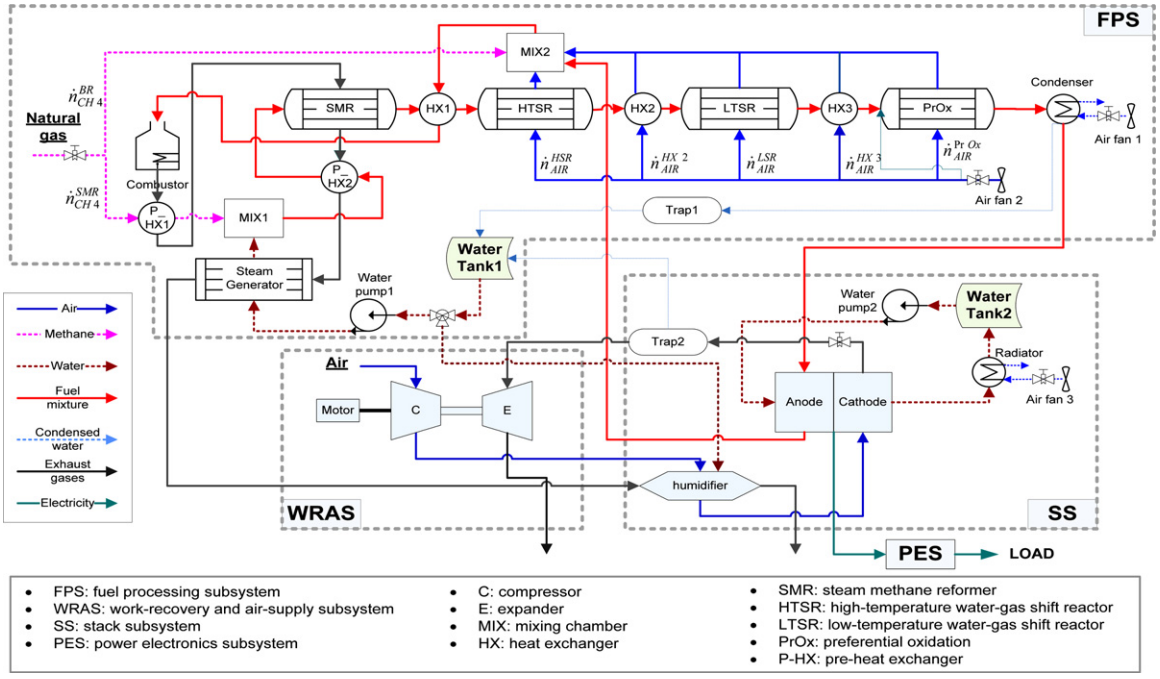

Fig. 2. Proposed non-optimized 5 kWe PEMFC system configuration.

high-/low-temperature water–gas shift reactors (HTSR/LTSR) and a preferential oxidation (PrOx) reactor.

As to the SS, a standard PEMFC stack based on Du Pont's Nafion™ is used which requires humidification, temperatures not in excess of 80 °C, and levels of CO not in excess of 10 ppm to avoid poisoning of the electrochemical catalyst. Thermal management in the SS is addressed by integrating the PEMFC stack with a water cooling cycle that controls the operating temperature of the stack.

The WRAS plays a significant role in the energy integration of the whole system. It consists of a compressor, an expander, and a motor. The compressor provides compressed air to the fuel cell stack and other balance of plant components and is driven by an expander and motor. An electric motor is used to supply additional power to the compressor in case the power extracted from the expander is not enough to run the compressor.

2.2. Subsystem modeling

2.2.1. SS

A semi-empirical, one-dimensional approach based on Ceraolo et al. [3] is used to model both the steady state and transient behavior of a single PEMFC as well as fuel cell stack. Each cell utilizes an H_2-rich gas mixture as the fuel and air as the oxidant, both humidified. The stack size (i.e., the number of cells and cell dimensions) is determined via an optimization process, which results in a system and set of components that meet the power demands and design objectives. The temperature of the fuel cell stack is assumed to be uniform (a good assumption as the temperature variation across the stack is relatively small) and is used to determine the flow rate of the stack cooling water used to maintain this stack temperature. The water vapor contained in the reactant mixtures in the pores of the cathode-side gas diffusion and electrode-catalysts layers is assumed to be in equilibrium with the surrounding liquid phase so that, consequently, the partial water pressure is uniform throughout these layers. Furthermore, the membrane electrolyte is assumed to be saturated completely with water so that its conductivity is only a function of temperature.

The current that is created by these electrochemical reactions depends directly on the potential difference between the carbon support for the catalyst and the polymer material surrounding the carbon supported catalyst as well as on the reactant concentrations. The reaction current density j_r can be expressed by the Butler–Volmer equation as

$$j_r = j_0 A_r \left[\frac{p_1}{p_1^0} \frac{[H^+]}{[H^+]_0} \exp\left(\frac{\alpha n F}{RT}\eta\right) - \exp\left(-\frac{(1-\alpha)nF}{RT}\eta\right) \right] \quad (1)$$

where $[H^+]$ is the bulk flow proton concentration, $[H^+]_0$ the reference proton concentration, η the voltage overpotential due to activation and concentration losses, α the transfer coefficient, n the number of electrons of the elementary electrochemical reaction, A_r the effective catalyst area per unit geometric area, and j_0 the exchange current density. The cell current density, j, is the sum of the reaction current density, j_r, and the charge storage which represents stored charge in the electrical double layer at the interface between the catalyst layer and the diffusion layer, i.e.,

$$j = j_r + C_{dl}\frac{\partial \eta}{\partial t} \quad (2)$$

where C_{dl}, the double layer capacitance, is assumed constant.

Ceraolo et al. [3] propose the following semi-empirical expression for the exchange current density:

$$j_0 A_r = j_{0l} A_{r0} \left\{ 1 + \left[\exp\left(\frac{\eta_b}{b_l} - \frac{\eta_b}{b_h}\right) - 1 \right] u(\eta - \eta_b) \right\} \times \exp(-a_1 j - a_2 j^5) \quad (3)$$

With Eqs. (2) and (3), transient behaviors of the cell current density can be calculated as a function of time.

2.2.2. WRAS

A screw type compressor and expander are selected for the WRAS. A screw compressor can provide a high discharge pressure at low mass flow rates and low speeds and also provides the oil-free output required by fuel cell systems. Therefore, even though screw compressors are more expensive than other typical

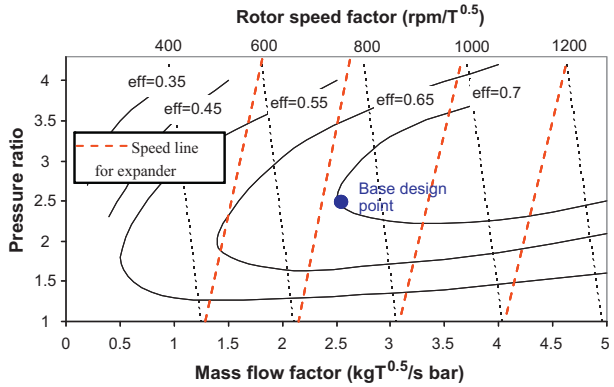

Fig. 3. Screw compressor performance map [8].

compressors, they are a better choice for small scale fuel cell systems. The compressor work rate is given by

$$\dot{W}_C = \dot{m}_{C,air} c_p \frac{T_C^{in}}{\eta_C} \left[\left(\frac{p_C^{out}}{p_C^{in}} \right)^{((\kappa-1)/\kappa)} - 1 \right] \quad (4)$$

where $\dot{m}_{C,air}$ is the mass flow rate, c_p the specific heat, T_C^{in} and T_C^{out} the inlet and outlet temperatures, p_C^{in} and p_C^{out} the inlet and outlet pressures, η_C the compressor efficiency, and κ the specific heat ratio. Any mechanical efficiency or leakage is ignored in this model. The compressor efficiency varies according to the flow rate and the pressure ratio. When it is available, dynamic operation of a compressor can be correctly described.

For partial loads, the map in Fig. 3 cannot be used directly for the fuel cell system because this map is for a 250 kWe system. In order to describe the appropriate operation of the compressor for the 5 kWe PEMFC system developed in this work, the map is scaled down by using scaling factors for the mass flow rate and pressure ratio as follow:

$$N_C = f(p_C SF_C^p, \dot{m}_C SF_C^m) \quad (6)$$

$$\eta_C = f(p_C SF_C^p, \dot{m}_C SF_C^m) \quad (7)$$

where $SF_C^m (= p_C^{B\cdot D}/p_C^{design})$ is the scaling factor for the pressure ratio and $SF_C^m (= \dot{m}_C^{B\cdot D}/\dot{m}_C^{design})$ that for the mass flow rate. $p_C^{B\cdot D}$ and $\dot{m}_C^{B\cdot D}$ are the base design point pressure ratio and mass flow rate factor, respectively. p_C^{design} and $\dot{m}_C^{design}$ are the design pressure ratio factor and mass flow rate factor determined by the optimization. The expander and DC motor designs implemented in the same way are described in detail in Kim [2].

The compressor and expander are connected via a single shaft so that the extracted power of the expander transfers to the compressor. The DC motor and compressor are linked through a gear drive as shown in Fig. 4. The required load on the motor, $\dot{W}_M$, is given by

$$\dot{W}_M = \dot{W}_C - \dot{W}_E \quad (8)$$

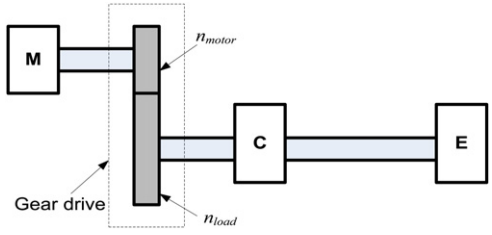

Fig. 4. Schematic of linkages between WRAS components.

Table 1
Economic assumptions for the economic analysis.

	Parameter	Values
N_{units}	Production volume	500,000
h	Operating hours per year	7920
N_{year}	Life time (years)	10
f_{main}	Maintenance factor per year	0.1 (10%)
I_{amor}	Interest rate per year	0.05 (5%)

where $\dot{W}_E$ is the work recovered by the expander. It is through the motor power that the transient modeling of the WRAS is accomplished via both a transient electrical and a transient torque balance on the motor.

2.2.3. FPS

Due to its complex structure, the FPS model requires a large amount of information to describe its kinetic characteristics, transient behavior, and design procedures which cannot be repeated here due to space limitations. Thus, the reader is referred to Kim [2] for more details.

3. Economic analysis

Although there are many available cost models for a variety of energy systems, it is difficult to find appropriate ones for small scale energy systems like the 5 kWe PEMFC system considered here. Moreover, even available cost models for small scale systems usually show significant discrepancies between the real market prices and the predicted prices. Using unrealistic cost models prejudice the system optimization results. Therefore, it is necessary to establish and use appropriate cost functions for the optimization process. In this study, cost functions for the 5 kWe PEMFC system are obtained from several different literature sources and modified by comparing them to real market prices. Table 1 summarizes some assumptions for the economic analysis. In addition, the natural gas price is obtained from the Energy Information Administration [4], and an average residential price of 13.75$ kft^{-3} is used for evaluating the operating costs. Details of the cost functions are given in Kim [2].

4. Optimization strategy

4.1. Multi-level optimization strategy

Conceptually, the decomposition process is placed in between the deterministic model and the optimizer as shown in Fig. 1. Decompositions in the multi-level approach can be achieved in four ways, i.e., disciplinary, conceptual, time, and physical decomposition [1]. In this study, physical decomposition is employed. Various physical decomposition techniques have been introduced in the literature and, in general, can be classified as methods of either local-global optimization (LGO) or iterative local-global optimization (ILGO). A dynamic version of the latter also exists designated as DILGO. Both ILGO and DILGO have been developed and their effectiveness validated in energy system synthesis/design and operation/control optimization by Munoz and von Spakovsky [5], and Rancruel and von Spakovsky [6].

4.1.1. DILGO and coupling function definition for the dynamic PEMFC system optimization under uncertainty

In order to apply the DILGO approach to the dynamic PEMFC system optimization problem, the system is decomposed into sub-systems connected by coupling functions. The decomposition coincides with the three subsystems described above (i.e., the SS, FPS, and WRAS), which are used as the basis for replacing the

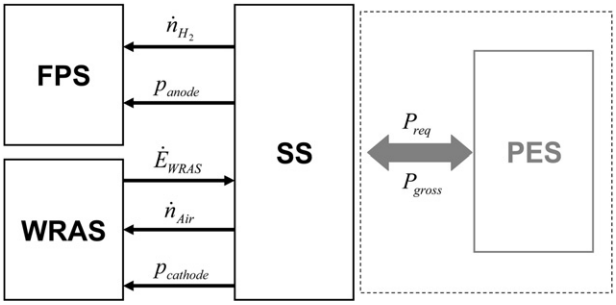

Fig. 5. Subsystem boundaries and coupling functions.

system-level optimization problem based on system total life cycle cost with three system-level, unit-based (SLUB) optimization sub-problems.

The system configuration in Fig. 2 is used as the initial configuration during the synthesis/design and operation/control optimization. Each subsystem boundary and the set of coupling functions used here, which represent material/energy flows or required operating conditions between subsystems, are depicted in Fig. 5. Although the PES is not modeled here, the SS and the PES are coupled by a controller to make the output power P_{gross} from the SS meet the power requirement P_{req} of the load demand. Five coupling functions are defined for the SLUB optimizations: the anode and cathode side pressures p_{anode} and $p_{cathode}$, the hydrogen flow rate $\dot{n}_{H_2}$ from the FPS, the air flow rate $\dot{n}_{Air}$ from the WRAS, and the motor parasitic power $\dot{E}_{WRAS}$.

The SS can be considered as the main subsystem of the PEMFC system because the FPS and the WRAS are run to satisfy the SS requirements (i.e., pressure, hydrogen and air flow rates) for a given load demand. To generate the gross electric power for a specific load and the required parasitic power $\dot{E}_{WRAS}$, the SS requires a certain amount of hydrogen and air (i.e., $\dot{n}_{H_2}$ and $\dot{n}_{Air}$) as well as operating pressure to minimize the total life cycle cost. These required hydrogen and air flow rates and pressure become the base profiles for conducting the SLUB optimizations of the dynamic FPS and WRAS. Even though stack temperature is also an important operating parameter, inlet temperatures of the air and hydrogen are not considered as coupling functions because these temperatures are managed by controllers so that they are not affected by the other subsystems.

To evaluate and quantify the uncertainty effects on system development, three uncertainty factors (i.e., with respect to the load profile, the cost functions, and certain inequality constraints (e.g., that on the CO concentration)) are considered for the optimization. For example, the total life cycle cost can be expressed in terms of expected total life cycle cost with a certain range, i.e., it can be expressed by deviation of the expected total life cycle cost in terms of the standard deviation. The RSA method has been employed to quantify the uncertainties in the simulations since it shows high fidelity and efficiency for the large-scale dynamic simulation problems [2,7] without the large computational burdens imposed by traditional stochastic approaches such as, for example, Monte Carlo simulations.

The following sections provide a detailed formulation of the SLUB optimization sub-problem for each subsystem with considered uncertainties in the objectives and constraints.

4.1.2. SLUB optimization

Total life cycle cost based objective functions are defined for the SLUB optimization sub-problems and summarized in Table 2. For example, the vector of equality constraints $\vec{H}_{FPS}$ represents the thermodynamic, kinetic, and geometric models of the FPS and the vector of inequality constraints $\vec{G}_{FPS}$ the physical limitations on the FPS such as the limit on CO concentration. Eq. (9c) indicates that the coupling functions $\dot{n}_{H_2}$ and p_{anode} must take the values which are found by solving the previous SS SLUB optimization sub-problem. Thus, the FPS SLUB optimization sub-problem is solved by fixing the inputs and optimizing the output, i.e., in this case the natural gas required.

Eq. (9) is the objective function for the SLUB optimization of the FPS. The SLUB objective function C'_{FPS} consists of contributions from the FPS (i.e., the capital cost C_{FPS} (or capital investment cost for the life cycle) of the FPS and the cost of fuel consumed C_{oper}), the optimum values for the capital costs of the SS C^*_{SS} and WRAS C^*_{WRAS} obtained from solving sub-problems (11) and (12), and the variation of the total life cycle cost in terms of its standard deviation (i.e., $C^{FPS}_{total,UNC}$). This standard deviation is expressed by Eqs. (9a) and (9b). C^{FPS}_{UNC} captures uncertainties in the SLUB optimization of the FPS based on uncertainties in the cost functions (i.e., purchase cost) of the FPS, load profile (i.e., variations in the hydrogen requirement), and fuel cost. C^{SS*}_{UNC}, C^{WRAS*}_{UNC} and C^{SS*}_{UNC} represent unit-level uncertainties obtained from the previous SLUB optimizations of the WRAS and SS using Eqs. (11b) and (12b). Operating cost defined as Eq. (10) represents total hydrogen requirement which is described in terms of cost. In order to estimate the life cycle operating cost required, the hydrogen consumption rate must be integrated over the entire operating time. This fuel consumption rate is described as a dynamic load profile and is dealt with in more detail in Section 4.2.

As to the inequality constraint for the CO concentration in the FPS SLUB optimization, G_{CO} is the mean value of the CO concentration of the reformate gas after the PrOx and G^{SD}_{CO} is the standard deviation of this CO concentration. By multiplying the standard deviation by 2, a 95% confidence interval for the CO concentration can be described. In addition, the parameters ν_{load}, ν_{fuel}, and ν_{COST} are the variances of the load profile, fuel cost, and purchase cost. An 8% standard deviation of the load profile and of the fuel cost and a 10% standard deviation of purchase cost are assumed, and all probabilistic distributions of the uncertainty sources are assumed as normal distributions.

Finally, a sequential scheme for the DILGO optimization approach for the PEMFC system synthesis/design and operation/control under uncertainty is proposed as shown in Fig. 6. The DILGO procedure is repeated until a set of predefined limits (0.1% in this study) on the SLUB optimizations are reached. Furthermore, note that the optimal control architecture and its control gains can be determined as part of an energy system synthesis/design and operation/control optimization problem. Wang [8] has done this for the optimal control architecture design of this PEMFC system based on a state-space control for a set of multi-input, multi-output (MIMO) controllers. In this work, the controller and control gains for each subsystem are obtained from Wang [8] where the gains are obtained from a set of preliminary subsystem-level optimizations by Wang.

4.2. Load profile

In order to conduct the optimization of the proposed dynamic PEMFC system, a dynamic load profile for a 5 kWe residential building is required. For this purpose, daily electricity consumption profiles of residential buildings in 2006 are obtained from Southern California Edison, and the mean and standard deviation of the load profiles are determined. In this study, it is assumed that the power demands during the summer and winter seasons are the most critical for system operation because more power is required during these seasons compared to the spring and fall. Therefore, a two-day load profile for the system optimization is developed in which half of the load profile represents the summer and the other

Table 2
Objective function definition of the SLUB optimization sub-problem for each subsystem.

Objective function (minimize)	Constraints	Uncertainty terms
FPS		
$C'_{FPS} = C_{FPS} + C_{oper} + C^{FPS}_{total,UNC} + C^{*}_{SS} + C^{*}_{WRAS}$ (9)	$\vec{H}_{FPS} = 0$ $\vec{G}_{FPS} \le 0$	$C^{FPS}_{total,UNC} = \sqrt{C^{FPS}_{UNC} + C^{SS*}_{UNC} + C^{WRAS*}_{UNC}}$ (9a)
where $C_{oper} = C_{NG} \int_{t=0}^{N_{year}} \dot{n}_{NG}\, dt$ (10)	$\begin{bmatrix} \dot{n}_{H_2} - \dot{n}^{*}_{H_2} \\ p_{andoe} - p^{*}_{anode} \end{bmatrix} = 0$	$C^{FPS}_{UNC} = \left(\frac{C^{FPS+}_{total,load} - C^{FPS-}_{total,load}}{2\delta^{FPS}_{load}}\right)^2 \nu^{FPS}_{load} + \left(\frac{C^{FPS+}_{total,fuel} - C^{FPS-}_{total,fuel}}{2\delta^{FPS}_{fuel}}\right)^2 \nu^{FPS}_{fuel} + \left(\frac{C^{FPS+}_{total,COST} - C^{FPS-}_{total,COST}}{2\delta^{FPS}_{COST}}\right)^2 \nu^{FPS}_{COST}$ (9b)
	$G_{CO,95\%} = G_{CO} + 2G^{SD}_{CO} \le 10$	$G^{SD}_{CO} = \sqrt{\left(\frac{G^{FPS+}_{CO,load} - G^{FPS-}_{CO,load}}{2\delta^{FPS}_{load}}\right)^2 \nu^{FPS}_{load}}$ (9c)
SS		
$C'_{SS} = C_{SS} + C^{SS}_{total,UNC} + C^{*}_{FPS} + C^{*}_{WRAS} + C^{*}_{oper} + \int_{t=0}^{T} \dot{\lambda}_{H_2} \Delta\dot{n}_{H_2}\, dt + \int_{t=0}^{T} \dot{\lambda}_{p_{anode}} \Delta p_{anode}\, dt + \int_{t=0}^{T} \dot{\lambda}_{Air} \Delta\dot{n}_{Air}\, dt + \int_{t=0}^{T} \dot{\lambda}_{p_{cathode}} \Delta p_{cathode}\, dt$ (11)	$\vec{H}_{SS} = 0$ $\vec{G}_{SS} \le 0$	$C^{SS}_{total,UNC} = \sqrt{C^{SS}_{UNC} + C^{FPS*}_{UNC} + C^{WRAS*}_{UNC}}$ (11a)
	$[\dot{E}_{WRAS} - \dot{E}^{*}_{WRAS}] = 0$	$C^{SS}_{UNC} = \left(\frac{C^{SS+}_{total,COST} - C^{SS-}_{total,COST}}{2\delta^{SS}_{COST}}\right)^2 \nu^{SS}_{COST}$ (11b)
WRAS		
$C'_{WRAS} = C_{WRAS} + C^{WRAS}_{total,UNC} + C^{*}_{SS} + C^{*}_{FPS} + C^{*}_{oper} + \int_{t=0}^{T} \dot{\lambda}_{\dot{E}_{WRAS}} \Delta\dot{E}_{WRAS}\, dt$ (12)	$\vec{H}_{WRAS} = 0$ $\vec{G}_{WRAS} \le 0$	$C^{WRAS}_{total,UNC} = \sqrt{C^{WRAS}_{UNC} + C^{SS*}_{UNC} + C^{FPS*}_{UNC}}$ (12a)
	$\begin{bmatrix} \dot{n}_{Air} - \dot{n}^{*}_{Air} \\ p_{cathode} - p^{*}_{cathode} \end{bmatrix} = 0$	$C^{WRAS}_{UNC} = \left(\frac{C^{WRAS+}_{total,Air} - C^{WRAS-}_{total,Air}}{2\delta^{WRAS}_{Air}}\right)^2 \nu^{WRAS}_{Air} + \left(\frac{C^{WRAS+}_{total,COST} - C^{WRAS-}_{total,COST}}{2\delta^{WRAS}_{COST}}\right)^2 \nu^{WRAS}_{COST}$ (12b)

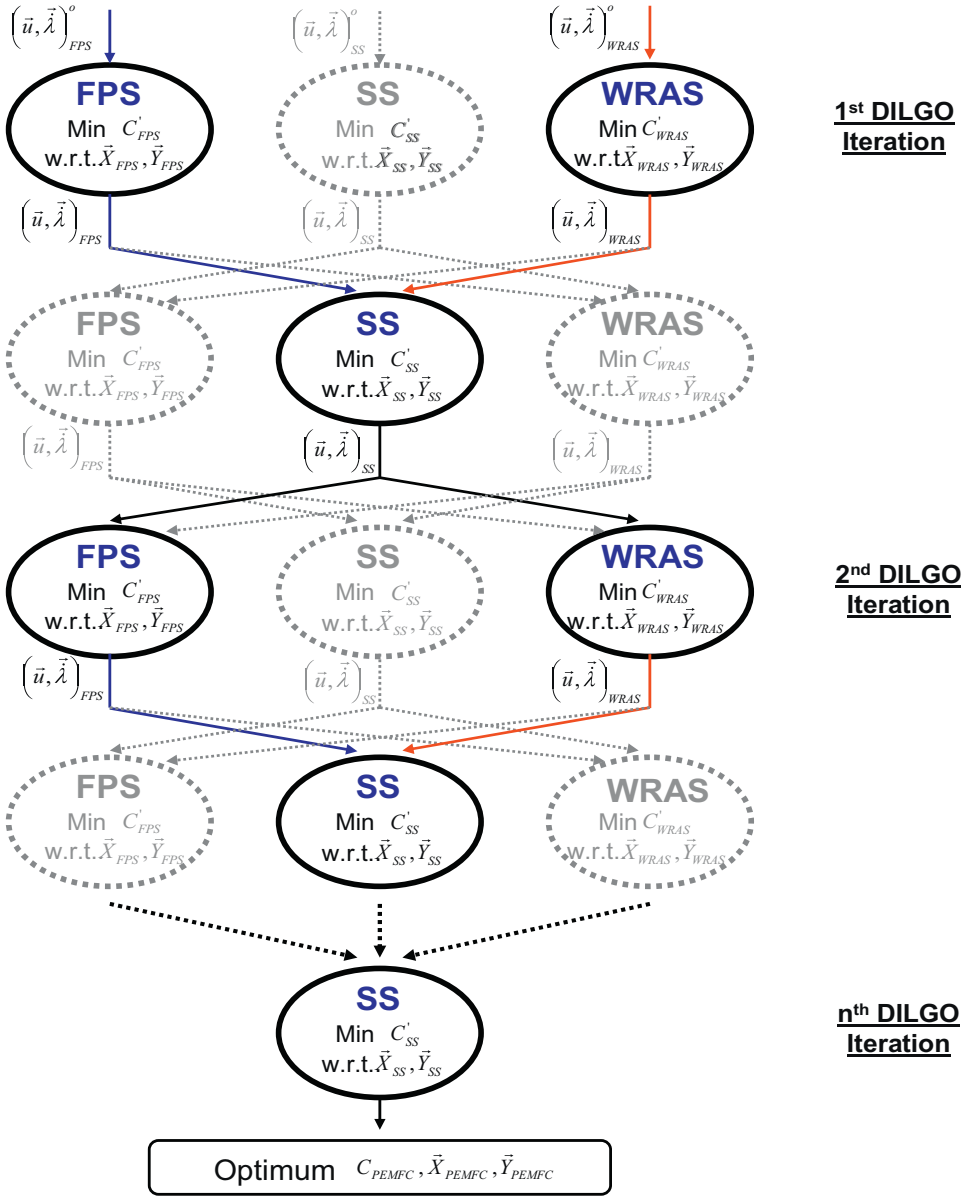

Fig. 6. Sequential computational scheme for the DILGO strategy.

the winter. Fig. 7 describes this 48-h load profile. In order to facilitate the calculation process, the peak point on the load profile is shifted to the starting point. That is why the 0th hour and 24th hour power demands are different in Fig. 7. As seen in the figure, the mean profile represents the real power consumed during the summer and winter, and the modified profile is a simplified version of the mean used for the optimization process. Day-to-day variations are described as uncertainties in the power demand of the mean load profile. Furthermore, to accommodate operation over a whole year, the modified 48-h profile is multiplied by 182. Of course, this yearly profile does not result in one, which accurately reflects the off-seasons of spring and fall since it simply extends the winter and summer seasons from a 6-month to a 12-month period. Nonetheless, it is used for the purpose of guiding the optimization towards a synthesis/design more conservative than might occur if the spring and fall seasons had been employed for the second six-month period.

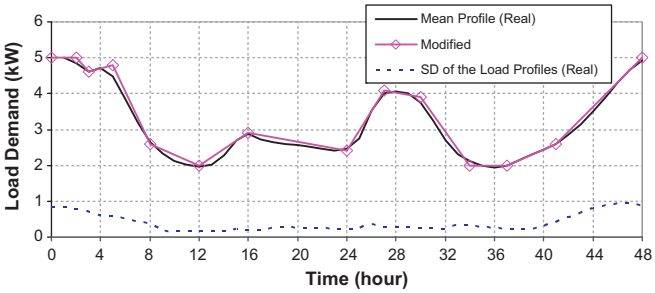

Fig. 7. Electricity demand profile and its variance over 48 h.

5. Results and discussion

5.1. Multi-level optimization results

The PEMFC life cycle costs and the uncertainties on these costs for each iteration of the DILGO approach are presented in Figs. 8 and 9. Via the DILGO process, the optimum cost of each

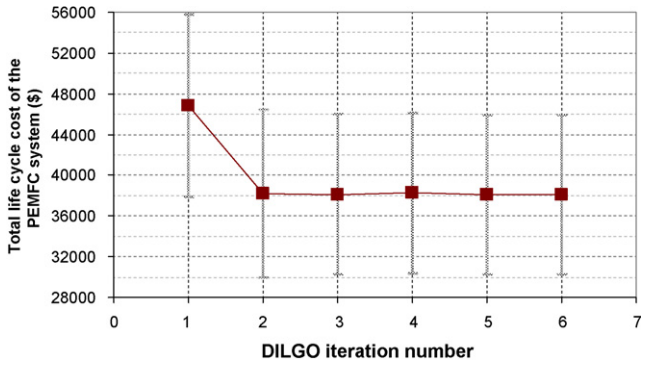

Fig. 8. Change in the total life cycle cost of the PFMFC system during the DILGO procedure with a 95% confidence interval.

subsystem is obtained and the optimum operating cost for the entire life time is also determined via the dynamic load profile. Fig. 8 presents the total life cycle cost, while Fig. 9 shows the optimum costs of the capital for each subsystem and the operating cost for each iteration. The DILGO procedure continues until improvement in the total life cycle cost is below 0.1%. The global optimum value for the total life cycle cost of the PEMFC system obtained during the 6th iteration of the DILGO procedure is $38,077 with a standard deviation of $3932. Thus, the optimum total life cycle cost of the PEMFC system is expressed as $38,077 ± $7864 with a 95% confidence interval. Uncertainties in the capital cost of each subsystem and the operating cost are presented in Fig. 9 using error bars. Preliminary studies [7] indicated that the mean values of the optimum total life cycle cost of the PEMFC system showed little difference whether or not the uncertainty terms were included. However, uncertainties on the constraints did significantly affect the optimization results. In particular, uncertainty considerations with regard to the CO concentration led to different results for the SLUB optimization of the FPS. That effect was taken into account in the optimization results in this paper. This uncertainty effect on optimization is explained in detail by the authors in Kim [2] and Kim et al. [7]. Readers are referred to those references for a better understanding of the uncertainty effects on PEMFC system development.

Significant improvements in the system-level objective function and capital costs of the subsystems are observed upon completion of the second DILGO iteration, and there are no significant improvements after the 4th iteration. The second DILGO iteration predicts the total life cycle cost of the PEMFC system to be $38,200 which is a 18.44% improvement over the first DILGO iteration, but there is only a 0.26% improvement from the second to the 6th DILGO iteration. It may appear that the optimization of the PEMFC is already completed after the second or the third DILGO iteration because there is little improvement after either. However, to determine whether or not the system-level optimization using DILGO has completed, the stabilization of all the coupling functions must be evaluated as well.

Fig. 10 depicts this stabilization. Fig. 10a and b presents the required hydrogen and air flow rate at the full load condition. Each point in the graphs coincides with the starting point of the dynamic profile in Fig. 7. The required hydrogen flow rate and the required air flow rate stabilize at 0.044 mol s^{-1} and 0.208 mol s^{-1} at the full load condition, respectively. Another coupling function, the motor parasitic power seen in Fig. 10c, oscillates with each DILGO iteration and begins to stabilize at around 420 W after the 6th DILGO iteration. As to the stack operating pressure, it is one of the coupling functions as well as one of the operation decision variables. The pressure plays an important role in PEMFC system operation because it affects PEMFC system performance and also determines the operating pressure of the FPS and WRAS. A final optimum operating stack pressure appears to stabilize at 2.22 bar in the 6th DILGO iteration as seen in Fig. 10d. Thus, it can be inferred from the figures that stabilized coupling functions may be obtained after one or two more DILGO iterations.

The global optimum synthesis/design and operation decision variable values of the PEMFC system appear in Table 3. The FPS SLUB optimization eliminates the first pre-heater, P_HX1, and the third

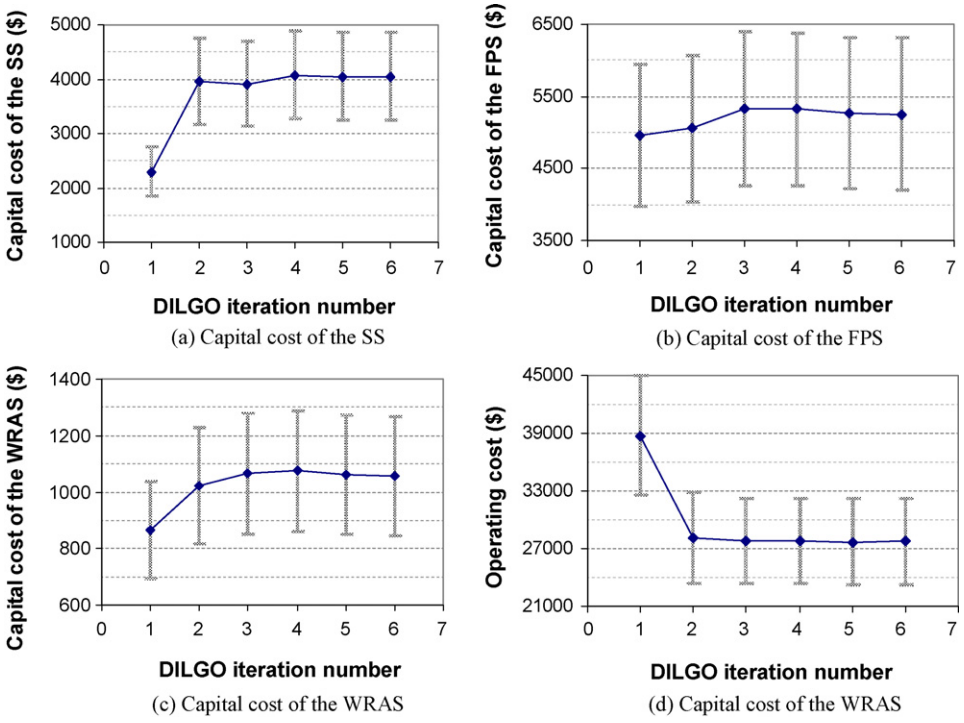

Fig. 9. Change in the capital costs of the SS, FPS, and WRAS and in the operating cost during the DILGO procedure with a 95% confidence interval.

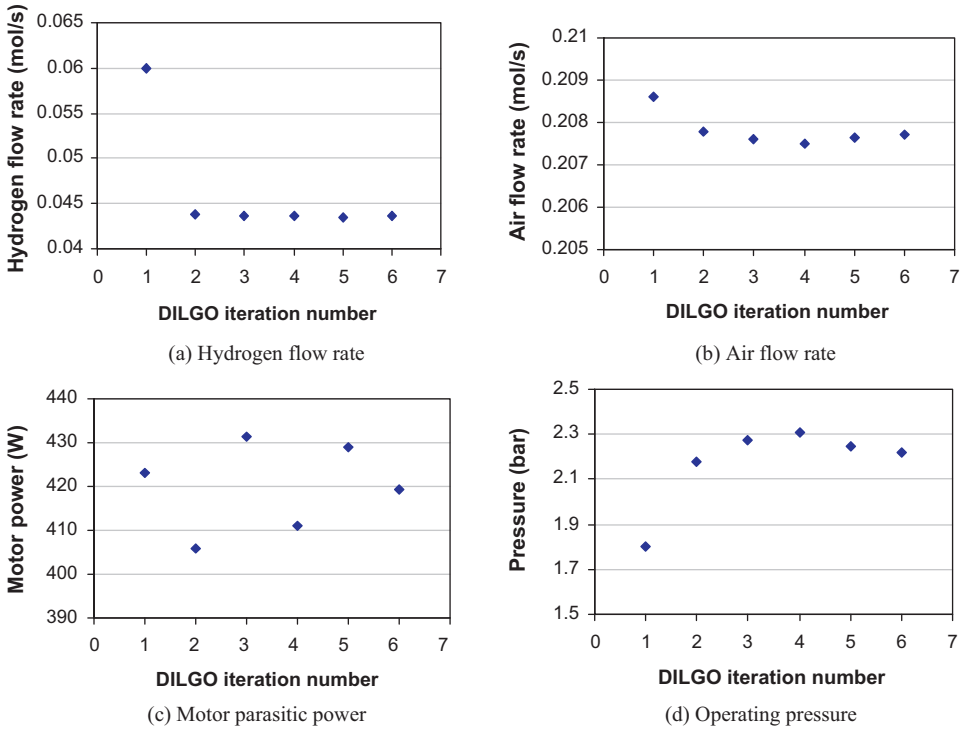

(a) Hydrogen flow rate (b) Air flow rate

(c) Motor parasitic power (d) Operating pressure

Fig. 10. Changing coupling functions during the DILGO procedure.

heat exchanger, HX3 from the initial configuration in Fig. 2. The optimal design of the SS predicts 0.127 m^2 for the single cell active area (3.7 m^2 of total cell active area), while the initial design of the SS has a single active area of 0.048 m^2 (2.0 m^2 total cell active area). The PEMFC stack efficiency increases with increasing stack (active area) size because the stack can operate at lower current densities as seen in Fig. 11. In this figure, the cell current density and hydrogen consumption rate decrease with increasing cell active area. Less cell current density produces higher cell voltage to generate the same amount of power. Thus, the larger size fuel cell stack consumes less hydrogen. This in turn reduces the operating cost of the PEMFC system. However, as the fuel cell stack size increases, the capital cost of the SS increases as well. Therefore, a compromise between the operating cost of the PEMFC system and the capital cost of the SS with regard to the stack size must be determined by the system-level optimization process. As seen in Table 3, this compromise results in a cell active area of 0.127 m^2 with the optimum number of cells being 29. Even though the larger cell size may cause some technical difficulties in terms of stack assembly, thermal management, and fuel distribution in the cell, these are not considered in this work because there is no available information about size limitations on stack design in the literature. If it becomes available, it must be taken into account as a constraint.

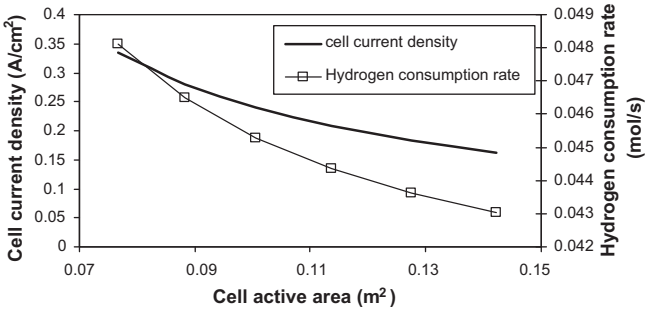

Fig. 11. Relationships between the single cell active area and current density and the H_2 consumption rate at full load.

The optimum purchase cost of each subsystem and its cost breakdown are presented in Table 4 based on a production rate of 500,000 manufactured units per year. Note that these costs are projected future costs which reflect a mature technology in which the major technical and lifetime issues have been largely resolved and the volume of units manufactured has reached levels sufficiently large to drop the cost of this technology to levels which make it competitive with more traditional technologies. With this qualification, the optimum purchase cost of the PEMFC system is $3720, and the optimum purchase costs of the FPS, SS, and WRAS make up 51%, 39%, and 10% of the system purchase cost, respectively. As shown in the table, the cost of the reactors (the SMR, HTSR, LSTR, and PrOx reactor) is around 62% of the optimum purchase cost of the FPS, that of the three heat exchangers (P_HX2, HX1, and HX2) 19%, and that of the auxiliary parts (e.g., valves, pipes, controllers, etc.) 17%. The remaining 2% is the steam generator. The stack purchase cost takes 82% of the optimum purchase cost of the SS, and 89% of that is for purchasing the electrodes which include the anode, cathode, and gas-diffusion-layers. The purchase cost of the auxiliary parts such as pipes, valves, and controllers for the SS represents 8% of the SS purchase cost. It should be noted that some of auxiliary parts for the SS are also common with the WRAS because both subsystems are coupled with each other via these valves and controllers. Thus, the purchase cost of these parts for the SS and WRAS is not considered in the purchase cost of the WRAS but in that of the SS.

5.2. Dynamic response of the SS

The dynamic responses of the cell current density and cell voltage over the 48 h of operation are depicted in Fig. 12. In this figure, the optimum responses are compared to the non-optimum (i.e., initial synthesis/design and operating conditions) responses. As seen in the figure, the optimum cell current density is lower than the

Table 3
Optimum synthesis/design and operation decision variable values.

Synthesis/design decision variables

Component	Decision variables	Initial value	Optimum value	Component	Decision variables	Initial value	Optimum value
FPS							
SMR	L^{SMR} (reactor length, m)	1.0	1.15	P_HX2	$L^{HX}_{P\_HX2}$ (heat changer plate length, m)	0.4	0.300
	d^{SMR}_{IN} (reactor tube diameter, m)	0.02	0.0237		$h^{HX}_{P\_HX2}$ (channel height, m)	0.004	0.0038
HTSR	L^{HTSR} (reactor length, m)	0.5	0.590		$N^{HX}_{P\_HX2}$ (Number of plates for each side)	4	4
	d^{HTSR}_{IN} (reactor tube diameter, m)	0.09	0.0663	HX1	L^{HX}_{HX1} (heat changer plate length, m)	0.25	0.540
LTSR	L^{LTSR} (reactor length, m)	0.6	0.680		h^{HX}_{HX1} (channel height, m)	0.004	0.0039
	d^{LTSR}_{IN} (reactor tube diameter, m)	0.09	0.0708		N^{HX}_{HX1} (number of plates for each side)	3	4
PrOx	L^{PrOx} (reactor length, m)	0.5	0.540	HX2	L^{HX}_{HX2} (heat changer plate length, m)	0.3	0.197
	d^{PrOx}_{IN} (reactor tube diameter, m)	0.08	0.0670		h^{HX}_{HX2} (channel height, m)	0.004	0.0039
SG	L^{SG} (steam generator tube length, m)	1.0	1.71		N^{HX}_{HX2} (number of plates for each side)	3	4
P_HX1*	$L^{HX}_{P\_HX1}$ (heat changer plate length, m)	0.2	N/A	HX3*	L^{HX}_{HX3} (heat changer plate length, m)	0.3	N/A
	$h^{HX}_{P\_HX1}$ (channel height, m)	0.004	N/A		h^{HX}_{HX3} (channel height, m)	0.004	N/A
	$N^{HX}_{P\_HX1}$ (number of plates for each side)	4	N/A		N^{HX}_{HX3} (number of plates for each side)	2	N/A
WRAS							
Motor	Tq^{Motor}_{design} (design torque, Nm)	3	2.10	Expander	$p^{Expander}_{design}$ (design pressure ratio)	2.0	2.17
	rpm^{Motor}_{design} (design rotational speed, rpm)	2400	1457		$\dot{m}^{Expander}_{design}$ (design mass flow factor)	0.1	0.076
Compressor	$p^{Compressor}_{design}$ (design pressure ratio)	2.2	2.18	*Unit:*	$\dot{m}^{Compressor}_{design}$ & $\dot{m}^{Expander}_{design}$ ($kg\,T^{0.5}/s\,bar$), Tq^{Motor}_{design} (Nm)		
	$\dot{m}^{Compressor}_{design}$ (design mass flow factor)	0.1	0.083				
SS							
Stack	L^{SS} (cell length, m)	0.218	0.357	Stack	N^{SS} (number of cells)	42	29

Operation decision variables

Variable	Initial value	Optimum value	Variable	Initial value	Optimum value
$\xi_{S/C}$ (steam-to-carbon ratio)	3.5	2.92	ξ^{HX3}_{AIR} (cooling air flow ratio of HX3)	0.12	N/A
ξ_{CH_4} (fuel feed ratio between SMR and combustor)	0.42	0.305	ξ^{PrOx}_{AIR} (cooling air flow ratio of PrOx)	0.40	0.300
ξ^{HTSR}_{AIR} (cooling air flow ratio of HTSR)	0.13	0.186	T^{HTSR}_{inlet} (inlet gas temperature of HTSR, K)	610	612
ξ^{HX2}_{AIR} (cooling air flow ratio of HX2)	0.28	0.365	p^{SS} (stack operating pressure, bar)	1.8	2.2
ξ^{LTSR}_{AIR} (cooling air flow ratio of LTSR)	0.07	0.149	*Component has been eliminated by the optimization		

Table 4
Optimum purchase cost based on 500,000 units/year.

SS ($)	
Stack	
Membrane	81.1
Bipolar Plate	46.2
Electrode	1046.7
Assembly	31.5
Stack purchase	1205.5
Humidifier	57.5
Cooling cycle	76.6
Auxiliary parts	114.8
SS purchase	**1454.4**

FPS ($)	
Reactors	1164.9
Steam Generator	41.4
Heat exchangers	365.7
Auxiliary parts	314.4
FPS purchase	**1886.5**

WRAS ($)	
Compressor	225.6
Expander	108.5
Motor	45.1
WRAS purchase	379.2

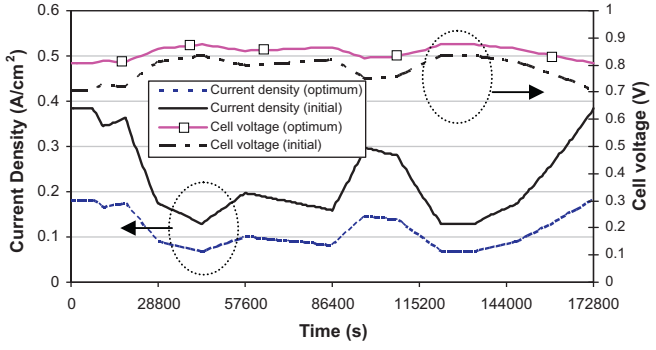

Fig. 12. Dynamic responses of the cell current density and cell voltage of the optimum and initial syntheses/designs.

non-optimum cell current density. Thus, the optimum cell voltage is higher than the non-optimum cell voltage to generate the same amount of electrical power. As explained in the previous section, the larger size fuel cell consumes less hydrogen, so operating costs are reduced. Through the system-level optimization, about 47% of the initial cell current density is predicted as the optimum cell current density. The optimum dynamic cell current density at the full load condition (at 0 s) is 0.18 $A\,cm^{-2}$ as compared to 0.38 $A\,cm^{-2}$ for the initial synthesis/design. At 40% of full load (at 43,200 s), it

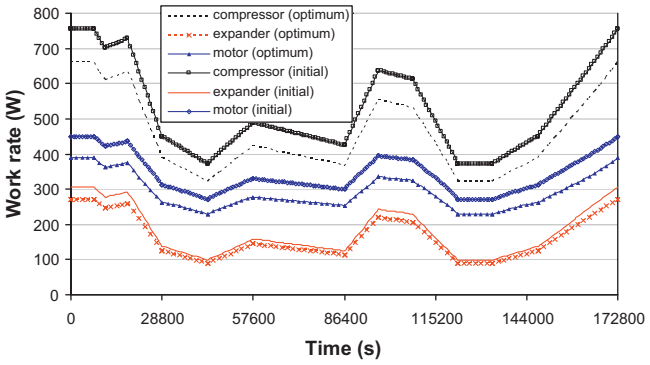

Fig. 13. Dynamic responses of the compressor, expander, and motor power for the optimum and initial designs.

is about 0.07 A cm^{-2} as opposed to the about 0.14 A cm^{-2} for the initial system.

5.3. Optimum design and dynamic responses of the WRAS

The optimum dynamic responses of the compressor, expander, and motor work rate are compared in Fig. 13 with the dynamic responses of the initial design over the 48 h of operation. The initial non-optimized design of the compressor requires 95 W more of power at the full load condition (at 0 s) and 40 W more at 40% of full load (at 43,200) than the optimum compressor. In the case of the expander unit, the initial non-optimized design of the expander recovers 35 W more at full load and 9 W more at 40% of full load than the optimum design. Therefore, taking into account the initial non-optimized motor design, the initial non-optimized design of the compressor needs an additional 61 W of work at full load and 42 W more at 40% of full load. This is the case because for the initial motor, which is non-optimized, the additional motor work rate is slightly higher than the difference between the additional work for the compressor (i.e., 95 W at full load and 40 W at 40% of full load) and the additional work recovered by expander (i.e., 35 W at full load and 9 W at 40% of full load).

The performance of the WRAS can also be expressed in terms of the work recovery rate which is the rate of the work recovered by the expander for the required work of the compressor. This is described in Fig. 14 which compares the work recovery rate of the optimum design and that of the initial non-optimized design. The optimum WRAS recovers about 41% with the required compressor work by the expander unit at full load, and about 28.5% at 40% of full load. The work recovery rate of the optimum WRAS is from 0.5 point percent (at full load) to 1.5 point percent (at 40% of full load) higher than that of the initial non-optimized WRAS as seen in the figure.

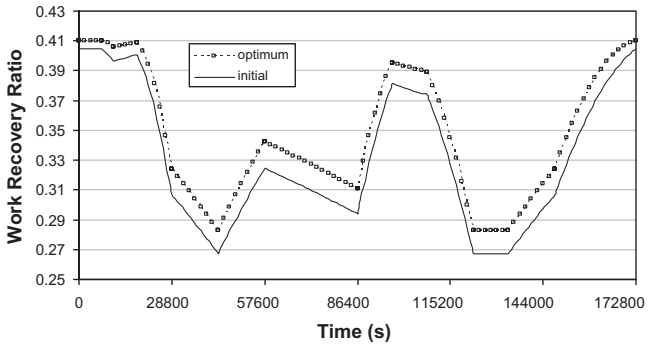

Fig. 14. Comparison of the optimum and initial work recovery ratio by the expander.

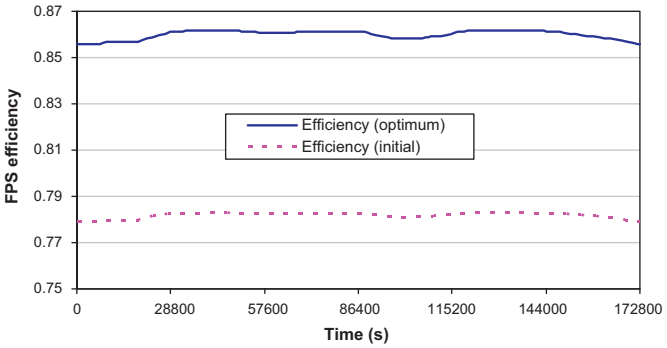

Fig. 15. Comparison of the optimum and initial (non-optimized) FPS efficiencies.

5.4. Optimum system efficiency

The efficiencies of the FPS, η_{FPS}, and the PEMFC, η_{PEMFC}, system are evaluated in this section and are defined as follow:

$$\eta_{FPS} = \frac{\dot{m}_{H_2} LHV_{H_2}}{(\dot{m}^{SMR}_{CH_4} + \dot{m}^{BR}_{CH_4})LHV_{CH_4} + \dot{m}^{BR}_{H_2} LHV_{H_2}} \quad (13)$$

$$\eta_{PEMFC} = \frac{\dot{E}_{net}}{(\dot{m}^{SMR}_{CH_4} + \dot{m}^{BR}_{CH_4})LHV_{CH_4}} \quad (14)$$

where $\dot{m}^{SMR}_{CH_4}$, $\dot{m}^{BR}_{CH_4}$, and $\dot{m}^{BR}_{H_2}$ are the methane flow rates to the SMR and burner and the hydrogen flow rate to the burner, respectively. Un-reacted hydrogen in the stack is fed into the burner. As a result of this, the overall system efficiency is improved. LHV_{CH_4} and LHV_{H_2} are the lower heating values of the methane and hydrogen, and $\dot{E}_{net}$ is the system net power.

Fig. 15 shows the dynamic optimum FPS efficiency over the 48 h of operation and compares it with that for the initial non-optimized FPS. The optimum FPS efficiency ranges from about 85.6 to 86.1% through the entire operating regime, while that for the initial non-optimized FPS varies from about 77.9 to 78.5%. Initially, a 0.42 fuel ratio is assumed and 0.305 is obtained from the optimization, which principally leads to an 8% efficiency enhancement of the FPS.

The optimum overall system efficiency of the PEMFC system shown in Fig. 16 is compared with that of the initial non-optimized PEMFC system. The optimum efficiency of the PEMFC system remains fairly steady at 46.5% throughout the operating regime, while that for the initial non-optimized system ranges from about 36 to 36.5%. Thus, the overall system efficiency increases by 10 percentage points through the optimization process. The main reason for the improvement is that the hydrogen fuel consumption of the optimum PEMFC system is reduced significantly compared to that for the initial non-optimized PEMFC system. The initial design of

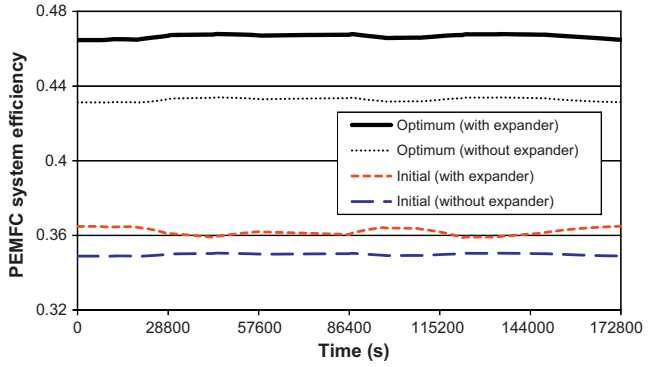

Fig. 16. Comparison of the optimum and initial (non-optimized) PEMFC system efficiencies with/without the expander unit.

the stack requires 0.0496 mol s^{-1} of hydrogen at full load but only 0.0436 mol s^{-1} for the optimum stack.

The effects of the work recovery unit using the expander are evaluated in terms of the PEMFC system efficiency in Fig. 16 as well. As seen in the figure, the system efficiency is enhanced by 3.4 percentage points by using the work recovery unit for the optimum PEMFC system, and by only 1.2 percentage points for the initial non-optimized PEMFC system.

6. Conclusions

Decomposition techniques are a very useful strategy for large-scale energy system optimization. In particular, the overall system model with its complex control architecture and very detailed component models results in a large computational burden and quite often simulation failure during a dynamic optimization. Fortunately, the optimization of the complex system model and control architecture can be treated as a set of approximate smaller unit (subsystem)-level optimization problems via a decomposition strategy such as DILGO. This physical decomposition approach is successfully applied to the synthesis/design and operation/control optimization of the dynamic PEMFC system, and the global optimum solution is found within 6 iterations by DILGO.

The optimum synthesis/design of the PEMFC system developed here shows a fairly steady and remarkably high overall system efficiency at 46.5% throughout the operating regime (i.e., full load to 40% of full load). The reason is that all design issues (i.e., synthesis/design and operation/control) are taken into account in one optimization problem so that all the optimum values are achievable. Moreover, system efficiency can be significantly enhanced by using the work recovery unit for the PEMFC system, and this study shows a 3.4 percentage points increase in system efficiency.

As to the operating cost, it dominates the life cycle cost of the PEMFC system during the optimizations. Thus, minimizing the fuel consumption rate of the system is of great importance. The optimum synthesis/design of the FPS plays a very important role in the entire PEMFC system synthesis/design and operation/control optimization problem because most of the additional fuel consumption in the PEMFC system occurs during the fuel processing (e.g., the hydrogen oxidation reactions in the preferential oxidation (PrOx) reactor, fuel for the combustor, poor reforming performance, etc.). The large cell active area also favors the reduction in the fuel consumption rate.

Finally, the approach presented here is an effective way of dealing in a single problem with dynamic fuel cell system synthesis/design and operation/control optimization under uncertainty. It is a general approach which can be applied to the optimal development of any energy system.

Acknowledgements

The authors would like to acknowledge the ASME as original publisher of a version of this paper in the proceedings of the 2008 International Mechanical Engineering Congress and Exhibition (IMECE 2008). This paper was submitted for publication to the *Journal of Power Sources* with permission of the ASME.

References

[1] D. Rancruel, Dynamic synthesis/design and operation/control optimization approach applied to a solid oxide fuel cell base auxiliary, Ph.D. Dissertation, Virginia Polytechnic Institute and State University, Blacksburg, VA, 2005.
[2] K. Kim, Dynamic proton exchanger exchange membrane fuel cell system synthesis/design and operation/control optimization under uncertainty, Ph.D. Dissertation, Virginia Polytechnic Institute and State University, Blacksburg, VA, 2008.
[3] M. Ceraolo, C. Miulli, A. Pozio, J. Power Sources 113 (2002) 131–144.
[4] Energy Information Administration, U.S. Natural Gas Prices, http://www.eia.doe.gov, 2006.
[5] J.R. Muñoz, M.R. von Spakovsky, An Integrated Thermoeconomic Modeling and Optimization Strategy for Aircraft/Aerospace Energy System Design, Efficiency, Costs, Optimization, Simulation and Environmental Aspects of Energy Systems (ECOS'00), Twente University, ASME, Netherlands, July 5–7 2000.
[6] D.F. Rancruel, M.R. von Spakovsky, Development and application of a dynamic decomposition strategy for the optimal synthesis/design and operational/control of a SOFC based APU under transient conditions, International Mechanical Engineering Congress and Exposition – IMECE 2005, ASME Paper No. IMECE2005-82986, New York, NY, November 2005.
[7] K. Kim, M. Wang, M. von Spakovsky, J. Nelson, Stochastic modeling and uncertainty analysis with multi-objective optimization strategies for the synthesis/design and operation/control of a PEMFC fuel processing subsystem, International Mechanical Engineering Congress and Exposition – IMECE 2008, ASME Paper No. IMECE2008-68065, Boston, MA, November 2008.
[8] M. Wang, Integration of state-space into the dynamic synthesis/design and operational/control optimization of a PEMFC system, Ph.D. Dissertation, Virginia Polytechnic Institute and State University, Blacksburg, VA, 2008.